Characterization of the Primary Photochemistry of Proteorhodopsin with Femtosecond Spectroscopy

Alisa Rupenyan,* Ivo H. M. van Stokkum,* Jos C. Arents,† Rienk van Grondelle,* Klaas Hellingwerf,*† and Marie Louise Groot*

*Department of Physics and Astronomy, Faculty of Sciences, Vrije Universiteit, 1081 HV Amsterdam, The Netherlands; and †Laboratory for Microbiology, Swammerdam Institute for Life Sciences, University of Amsterdam, 1010 WV Amsterdam, The Netherlands

ABSTRACT Proteorhodopsin is an ion-translocating member of the microbial rhodopsin family. Light absorption by its retinal chromophore initiates a photocycle, driven by *trans/cis* isomerization, leading to transmembrane translocation of a proton toward the extracellular side of the cytoplasmic membrane. Here we report a study on the photoisomerization dynamics of the retinal chromophore of proteorhodopsin, using femtosecond time-resolved spectroscopy, by probing in the visible- and in the midinfrared spectral regions. Experiments were performed both at pH 9.5 (a physiologically relevant pH value in which the primary proton acceptor of the protonated Schiff base, Asp^{97}, is deprotonated) and at pH 6.5 (with Asp^{97} protonated). Simultaneous analysis of the data sets recorded in the two spectral regions and at both pH values reveals a multiexponential excited state decay, with time constants of ~0.2 ps, ~2 ps, and ~20 ps. From the difference spectra associated with these dynamics, we conclude that there are two chromophore-isomerizaton pathways that lead to the K-state: one with an effective rate of $\sim(2\ \text{ps})^{-1}$ and the other with a rate of $\sim(20\ \text{ps})^{-1}$. At high pH, both pathways are equally effective, with an estimated quantum yield for K-formation of ~0.7. At pH 6.5, the slower pathway is less productive, which results in an isomerization quantum yield of 0.5. We further observe an ultrafast response of residue Asp^{227}, which forms part of the counterion complex, corresponding to a strengthening of its hydrogen bond with the Schiff base on K-state formation; and a feature that develops on the 0.2 ps and 2 ps timescale and probably reflects a response of an amide II band in reaction to the isomerization process.

INTRODUCTION

pRs are members of the large family of microbial rhodopsins (1). They are widely distributed in marine proteobacteria and spectrally tuned to the light climate in their oceanic environment, which has led to the evolution of blue and green variants. Their relative use of solar energy in the biosphere is probably significant (2). It seems that many of the planktonic prokaryotes in the photic zone of the oceans that do not contain a (bacterio)chlorophyll-based photosynthetic apparatus nevertheless exploit light by having acquired pR through lateral gene transfer (3).

Although it has been demonstrated that pRs function as light-driven proton pumps, their precise physiological role is still not completely clarified. Studies of pR expressed in *Escherichia coli* have shown that it allows *E. coli* cells to withstand environmental respiration challenges by harvesting light energy (4). It has been firmly established that green-light-absorbing pR, the subject of study of this investigation, functions as a light-driven proton pump. pRs with a blue-shifted absorption spectrum, however, show a significantly slower photocycle (5), and their tertiary structure, deduced from homology modeling, is closer to the structure of sensory rhodopsin II (6), suggesting a sensory function rather than a light-harvesting function. Absence of the presumed proton donor to the Schiff base in several genes encoding a microbial rhodopsin has recently led to the proposal of the existence of proteobacterial sensory rhodopsins (7).

Similar to bacteriorhodopsin, the absorption of light by pR's chromophore, a retinal molecule covalently linked to the apoprotein through a protonated Schiff base, initiates *E/Z* (or all-*trans* to 13-*cis*) isomerization of the chromophore. This leads to a series of thermal transitions during which the proton from the Schiff base is transferred to the counterion formed by Asp^{97}, Asp^{227}, and a bound water molecule (Fig. 1) (8–10). Additional residues from the corresponding complex counterion in bacteriorhodopsin, such as Arg^{82}, are conserved in pR (i.e., Arg^{94}). The Schiff base is reprotonated by a proton from Glu^{108}. However, pR lacks the ionizable residues corresponding to Glu^{194} and Glu^{204} of bacteriorhodopsin, thought to be involved in the proton release pathway at the extracellular surface, which leaves the exit route of the proton in pR uncertain. In blue pR, Asp^{227} was identified as an alternative second proton acceptor (6).

At pH values lower than the ambient pH of the organism (which is slightly alkaline), the absorption maximum of pR is red-shifted, and the M-intermediate, which has a deprotonated Schiff base, is absent from the photocycle (11). These changes have been attributed to a change in the protonation

Submitted September 5, 2007, and accepted for publication January 9, 2008.

Address reprint requests to Rienk van Grondelle, Dept. of Physics and Astronomy, Faculty of Sciences, Vrije Universiteit, De Boelelaan 1081, 1081 HV Amsterdam, The Netherlands. E-mail: rienk@nat.vu.nl.

Abbreviations used: pR, proteorhodopsin; VIS, visible; IR, infrared; DM, dodecyl-maltoside; EADS, evolution-associated difference spectra; ES1, ES2, ES3, first, second, third excited state; SADS, species-associated difference spectra; xpm, cross-phase modulation; K- and M-intermediate, first ground-state intermediate after photoisomerization and after Schiff base deprotonation, respectively; FTIR, Fourier transform infrared spectroscopy.

Editor: Janos K. Lanyi.

0006-3495/08/05/4020/11 $2.00

doi: 10.1529/biophysj.107.121376

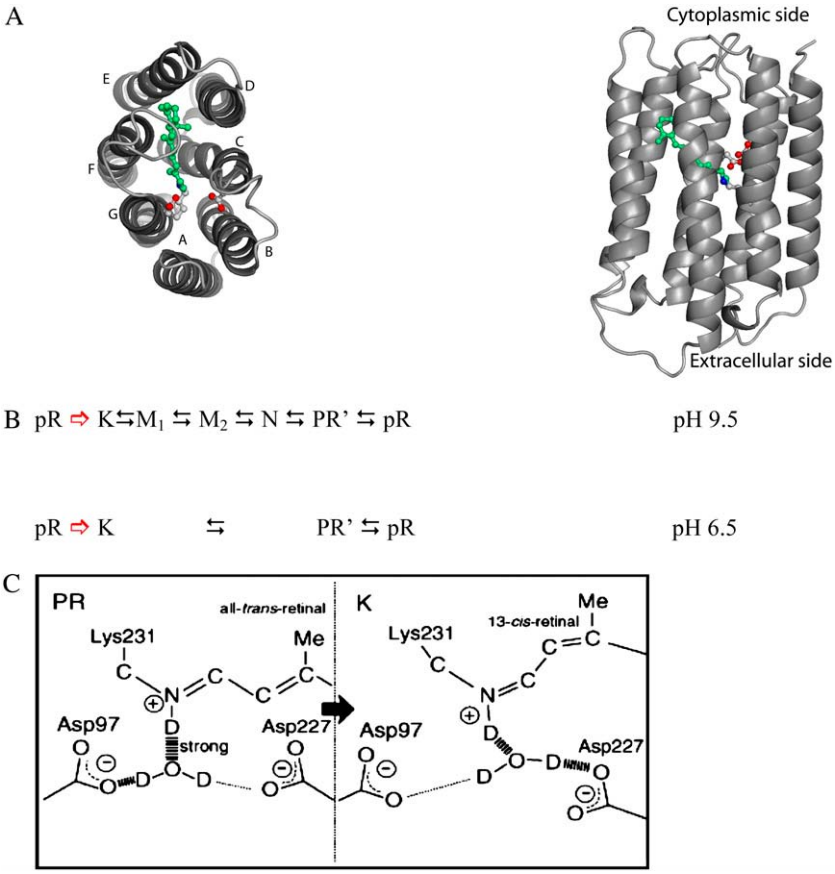

FIGURE 1 Key features of green pR. (*A*) Schematic representation of the spatial structure of pR, drawn as a ribbon diagram, with the retinal chromophore, Asp^{227} and Asp^{97}, that jointly form the complex counterion of the protonated Schiff base, drawn in ball-and-sticks: Top view (*left*) and side view (*right*). The letters A–G refer to the seven transmembrane helices of the protein. The figures were prepared with homology modeling (5). (*B*) Summary of the micro- to millisecond events in the photocycle of pR (essentially reproduced from Lakatos and Varo (50)). The open arrow represents photoactivation. (*C*) Model of the structural changes in the retinal-binding pocket of pR, accompanying the pR-to-K transition (deuterated sample), as deduced from low-temperature IR difference spectroscopy (reproduced with permission from Ikeda et al. (9)).

state of the primary proton acceptor Asp^{97}, which has a pK_a of ~7.2 (12). Remarkably, in pH-dependent photocurrent measurements on planar lipid bilayers at low pH after the absorption of two photons, proton pump activity with reversed directionality was reported to take place (13). Other investigators, however, reported absence of proton transport under acidic conditions (11,12,14).

The kinetics of the other intermediates in the photocycle of pR under acidic or alkaline conditions do not differ markedly (13), but changes in the kinetics of the primary photochemistry, the photoisomerization of the retinal chromophore, have been reported (15). Furthermore, the protein side chains surrounding the retinal chromophore play a crucial role in the selectivity and efficiency of the photoisomerization. As shown by FTIR spectroscopy, low pH and the D227N mutation drastically enhance the yield of the 9-*cis* photoproducts (14) at the cost of the 13-*cis* product formed under physiological conditions. Low-temperature FTIR studies showed that the D227N mutation strongly affects the N-D stretching vibration of the protonated Schiff base, whereas the effect of the N97D mutation on the Schiff base is negligible (9). Based on these studies, it has been proposed that Asp^{227} is the hydrogen bond acceptor of the protonated Schiff base in the photoisomerized K-state (see also Fig. 1).

According to Lenz et al. (16), the protonation state of the Schiff-base proton acceptor (Asp^{97}), which is deprotonated at high pH and becomes protonated with a pK_a of 7.2, affects the reaction rate and the quantum efficiency of the primary reactions in pR. In ultrafast optical absorption and fluorescence studies at acidic and alkaline pH, these authors observed a biphasic decay of the excited state with time constants of a few hundred femtoseconds and ~10 ps, respectively, which was interpreted with a ''branching reaction'' model, in which part of the molecules isomerize directly from the first excited state and another part isomerizes after a transition through a relaxed state. At high pH, the first pathway is preferred over the direct pathway. The reaction dynamics were observed to slow down in a study of the D97N mutant of pR, and therefore. altered steric interactions, induced by the change in pH, were proposed to also affect the kinetics (17).

In a recent time-resolved IR study of pR at pH 9.5, using a time window of 30 ps, by Amsden et al. (18), four kinetic components were identified in the temporal evolution of the vibrational spectra: 0.5 ps, 2 ps, 11 ps, and a long-lived component. Vibrational bands characteristic for all-*trans* to 13-*cis* isomerization were found to appear within 0.5 ps, whereas a ground state was observed to be populated after 2 ps. With isotope labeling, the authors identified a negative band at 1548 cm^{-1} as an amide II band, which bleached on a subpicosecond timescale. This was interpreted as a conformational change occurring almost at the same time as the isomerization of the chromophore.

Transient absorption spectroscopy in the visible part of the spectrum is, because of its excellent signal/noise ratio, well suited to provide information about the decay of the excited state of the retinal chromophore and the associated formation of photocycle intermediates. Transient vibrational absorption spectroscopy, however, provides more information with respect to the detailed structural changes of the retinal molecule and its immediate surroundings. Therefore, we have used a combination of ultra-fast VIS and IR spectroscopy to derive a unified, quantitative model for the initial dynamics in the structure of pR. Measurements were performed at two relevant ambient pH values, to observe the dynamic behavior of the vibrational isomerization marker bands and formation of the K-state, on the timescale from 100 fs to 1 ns. Simultaneous analysis of the different spectral regions has allowed us to propose a detailed reaction model and to characterize the differences observed at high and low pH.

MATERIALS AND METHODS

pR was isolated from *E. coli* UT5600/pBeta-caro/pKJ829-proteo, a strain kindly provided by Dr. K. H. Yung (Department of Life Science, Sogang University, Seoul, Korea). The pBeta-caro plasmid carries a chloramphenicol resistance marker and leads to the constitutive production of β-carotene. The pKJ829-proteo plasmid encodes ampicillin resistance, an L-arabinose-inducible retinal synthase, and an isopropyl-β-D-1-thiogalactopyranoside-inducible polyhistidine-tagged pR gene. pR formation is induced overnight at 30°C with 0.1% (w/v) L-arabinose plus 1 mM isopropyl-β-D-1-thiogalactopyranoside. Membranes containing holo-pR were isolated by resuspending harvested *E. coli* cells in ~1/100 culture volume of 20 mM Tris buffer, pH 7.5, containing 500 mM NaCl, 0.1% (w/v) DM, and 20 mM imidazole, after which cells are frozen.

After thawing and addition of 1 mg/ml lysozyme, 25 μg/ml DNase I, 25 μg/ml RNase, and a protease inhibitor cocktail, cells were disrupted by sonication. Cell debris was removed by low-speed centrifugation (10 min at $3000 \times g$), and the supernatant was solubilized in detergent (1.5% (w/v) DM) and slowly stirred overnight at 4°C. Next, the sample was centrifuged at low spin speed (see above) for 15 min to remove remaining aggregates, and pR was purified using a HisTrap FF crude column (GE Healthcare, Eindhoven, The Netherlands) in combination with an imidazole gradient. The protein was concentrated with YM-10 Centriprep (Amicon, Billerica, MA), and the imidazole was removed with a desalting column (GE Healthcare). Finally pR was eluted in 0.5 M NaCl, 0.1 % (w/v) DM, plus 25 mM glycine buffer at pH 9.5 or in a 25 mM MES buffer at pH 6.5, and concentrated (Microcon filters, Millipore, Bedford, MA).

Samples consisted of a highly concentrated protein solution contained between two CaF_2 windows, separated by a 20-μm Teflon spacer. The optical density of the sample was 0.25 at 518 nm for the sample at pH 9.5 and optical density 0.25 at 532 nm at pH 6.5. The respective absorption maxima are consistent with values reported in the literature for pR at pH 9.5 and 6.5 (13).

Data from high-performance liquid chromatography analysis of extracted chromophore (19) indicate that the isomeric composition of dark-adapted retinal from pR is 95% all-*trans* and 5% 13-*cis*; the same ratio was determined by FTIR studies (20). Therefore, significant contributions of a 13-*cis* photocycle in our spectra can probably be excluded, but the possibility was tested nevertheless by experiments with excitation at longer wavelengths. If a 9-*cis* isomer were present in the ground state or formed after repeated cycles of photoactivation of all-*trans* retinal, one would expect altered spectral characteristics in the mid-IR ~1550 cm^{-1}, corresponding to the C=C stretch of a 9-*cis* isomer and a blue shift of the absorption in the visible. When we excited pR with 550-nm light (i.e., red-shifted with respect to the normal excitation wavelength of 530 nm) to minimize any excitation of a possible 9-*cis* isomer, we did not find any significant changes in the resulting IR difference spectra (data not shown); nor was there any indication of a 9-*cis* species in the VIS pump-probe data.

The experimental setup consists of an integrated Ti:sapphire oscillator-regenerative amplifier laser system (Hurricane, SpectraPhysics, Mountain View, CA) operating at 1 kHz and at a central wavelength of 800 nm, producing 85-fs pulses of 0.7 mJ. Part of this 800-nm light was used to pump a noncollinear optical parametric amplifier to produce the excitation pulses with a center wavelength of 530 nm (used for both pH values) and an energy of 200 nJ, focused to a diameter of ~120 μm. A second portion of the 800-nm light was used to pump an optical parametric generator and amplifier with a difference frequency generator (TOPAS, Light Conversion, Vilnius, Lithuania) to produce the mid-IR probe pulses. These low-intensity probe pulses were spatially overlapped with the excitation beam in the sample. After overlap in the sample, the mid-IR probe pulses were dispersed in a spectrograph and imaged onto a 32-element mercury cadmium telluride detector (Infrared Associates, Orlando, FL). The polarization of the excitation pulse was set to the magic angle (54.7°) with respect to the IR probe pulses. A phase-locked chopper, operating at 500 Hz, ensured that every other shot the sample was excited, and an absorbance difference spectrum could be calculated. To ensure a fresh spot for each laser shot, the sample was moved by a home-built Lissajous scanner. The measurements were performed in a box flushed with dry air to reduce the interference of water vapor with the measurements. In a single experiment, a spectral probe window of ~200 cm^{-1} was covered. Therefore, three partly overlapping IR regions were measured to cover the spectral range from 1188 to 1600 cm^{-1}; experiments were repeated at least two times.

The vis/vis experiments were performed with the same setup, which was extended with an arm in which white light was generated in a 2-mm sapphire plate. This probe light was focused on the sample with the same lens used to focus the excitation pulse, dispersed on a spectrograph, and imaged onto one of the arrays of a double 256-element diode array (Hamamatsu Photonics, Hamamatsu, Japan). The diode array was read after every shot using a 16-bit ADC (Analogue Devices, Norwood, MA) and EDT CD 20 digital I/O board. The instrument response function was ~150 fs for both experiments. For the vis/vis experiment, the excitation wavelength was also set at 530 nm, and the excitation energy was also the same as in the VIS-pump/IR-probe experiments.

The data were subjected to global analysis (21). The xpm and scattering correction procedure was performed for the visible data by fitting and subtracting the xpm contributions for every time trace, measured under exactly the same conditions in the sample cell filled only with buffer.

The model structure of pR, derived with homology modeling described by Man et al. (5), contained orientations of amino acid side chains that sterically overlapped with the retinal chromophore (residues Trp^{73}, Trp^{172}, and Lys^{206}). Using the amino acid sequence of pR as input in the 3DJigsaw homology-modeling webserver (22), we identified the NMR structure of dark-adapted bacteriorhodopsin (Protein Data Bank code 1R84) (23) as a suitable template to improve the structural model of pR. This template, in combination with the sequence alignment obtained from 3DJigsaw, served as input for the SWISS-MODEL web server (24) and resulted in an improved model for the retinal binding pocket.

Structure representations were made with the program PyMol (De Lano Scientific, San Carlos, CA).

RESULTS

Transient absorption difference spectra in the 450–720 nm range

In Fig. 2 *A*, the absorption changes induced by excitation of the sample with a 60-fs laser pulse at 530 nm are shown for both pH 6.5 (*left*) and 9.5 (*right*). The dynamic spectral changes are initially characterized by a ground-state bleach and stimulated emission in the region of 550 nm to 720 nm,

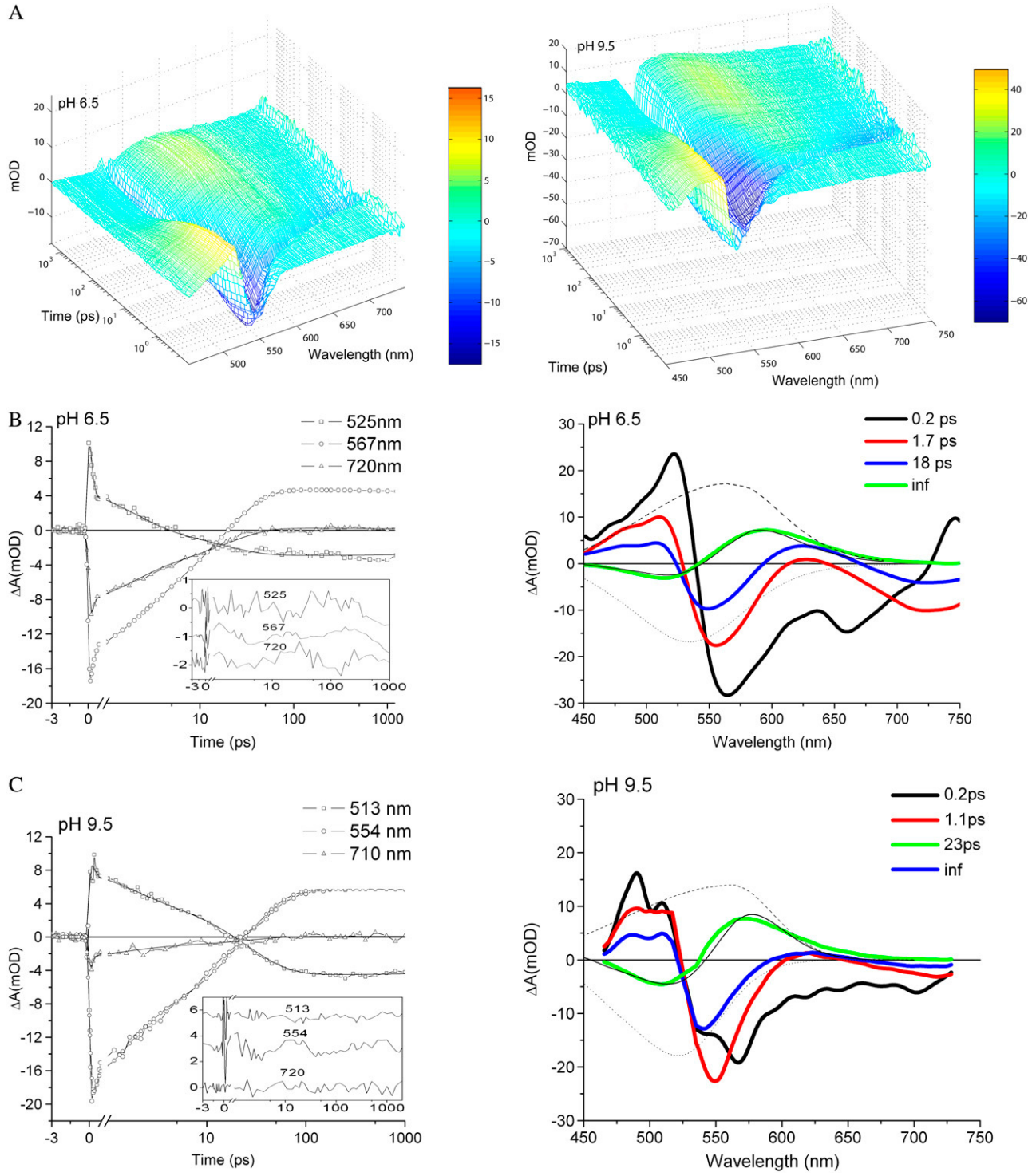

FIGURE 2 Results of VIS-pump/VIS-probe measurements of pR at pH 6.5 and pH 9.5. (*A*) Three-dimensional surface plots of the raw ultrafast transient absorption data at acidic (*left*) and alkaline pH (*right*); note the shift in stimulated emission (negative signal at 600–750 nm) during the first 10 ps. (*B*) Selected time traces and corresponding fits resulting from global analysis that show the absorption changes as a function of time (*left panel*) and EADS of pR at pH = 6.5, derived from a global analysis, based on a sequential model. The inset shows the residuals of the fit of the model to the measured time traces. (*C*) Selected EADS and time traces of pR at alkaline pH. The time constants associated with each EADS are given in the inset. Also indicated is a schematic representation of the bleached steady-state absorption (*dotted line*), the modeled product state absorption (*dashed line*), and the resulting difference spectrum (*solid line*).

excited-state absorption in the region $\lambda < 550$ nm that develops into a bleach ~525 nm and an induced absorption band at 575–580 nm at later delay times.

The time-dependent spectral evolution of the data is well described using a simple sequential scheme, with increasing exponential lifetimes of 0.2 ps, 1.7 ps, 18 ps, and a nondecaying component (for pH 6.5) and 0.2 ps, 1.1 ps, 23 ps, and a nondecaying component (for pH 9.5). The left-hand parts of Fig. 2, panels *B* and *C*, show selected time traces from different spectral regions with the residuals of the fit (*inset*). The EADS are shown in black, red, blue, and green, respectively (Fig. 2, *B* and *C*, *right panels*).

The earliest dynamics occur on a very fast timescale, on the order of the instrument response function. Therefore, we fixed the first component to 0.2 ps for both pH values. Clearly, the corresponding EADS also contains some coherent contributions from the temporal overlap of the pump and probe pulses. After the fast initial evolution, the absorption difference spectra show ground-state bleach peaking at ~550 nm, excited-state absorption in the region of 450–530 nm, and stimulated emission in the region of 650–720 nm, whereas a very small positive feature is present at ~625 nm (*red spectra*). Subsequently, with a time constant of 1–2 ps, the stimulated emission and the excited state absorption partially decay, which is accompanied by the growth of the positive signal at ~625 nm (*blue spectra*). After 18 ps at pH 6.5 (23 ps at pH 9.5), the excited state absorption further decays and develops into a negative signal peaking at ~510 nm, whereas the positive signal further develops into a band peaking at ~580 nm (~560 for the sample at pH 9.5). On the same timescale, the stimulated emission signal on the red side of this positive feature (675-750 nm) has decayed to zero. This final (*green*) spectrum (on the timescale of our experiment) can be attributed to the sum of the bleached ground state absorption and absorption resulting from product formation. Note that, in the spectra at delay times shorter than 20 ps, this ground-state bleaching was partially obscured by excited-state absorption at ~500 nm. The final spectrum, representing that of the K-state (10), can be well simulated with the sum of the ground-state absorption spectrum (peaking at 519 nm for pH 9.5 and 532 nm for pH 6.5, see *dotted lines* in Fig. 2) and a product absorption band peaking at 560 nm for pH 9.5 and 570 nm for pH 6.5 (see *dashed lines* in Fig. 2). Residuals resulting from the fit of the model to various time traces (see Fig. 1S, *A* and *B*, in the Supplementary Material, Data S1) show essentially no structure for both acidic and alkaline pH over the full range of delays and probe wavelengths. The resulting EADS accordingly provide a reasonable basis for comparison of the various phases of spectral evolution and the underlying dynamics.

Quantum yield of the initial photochemistry

An estimation of the quantum yield of K-formation can be made from the ratio of the bleached bands of the pR ground state and of the K-product band and the extinction coefficient of each state. Because to the best of our knowledge the extinction coefficient of retinal in the K-state of pR has not been determined, the ratio of the extinction coefficient of retinal in the ground state and in the K-state is assumed to be as in bacteriorhodopsin, a proton pump with a very similar photocycle (10), in which it is ~0.8 (25). Because the first spectrum may still contain some remains of the coherent artifact, we determine the quantum yield of the reaction from the ratio of the amplitudes of the 1-ps spectrum (*red spectrum* in Fig. 2) and the maximum of the green product absorption difference spectrum, corrected for wavelength according to the modeled K-spectrum and the steady-state spectrum of pR, respectively (*dashed* and *dotted lines* in Fig. 2, *B* and *C*). This procedure results in estimations of the quantum yield for pR at both acidic and alkaline pH of ~0.5, which is in line with the photoisomerization quantum yields of related photoactive proteins: 0.7 for bacteriorhodopsin (26) and 0.3 for photoactive yellow protein (27) and halorhodopsin (28). It should be noted, however, that because of the extensive overlap of the absorption spectra in the ground state, excited state, and product state, the estimation of the quantum yield using this method may not be very accurate. A further estimate of the quantum yield may be obtained from the rates of K-formation and ground-state recovery, as determined in a target analysis (see below).

Transient absorption difference spectra in the mid-IR

To gain further insight into the process of photoisomerization, we studied the vibrational absorbance changes in the mid-IR region, again on excitation at 530 nm. These data were also initially analyzed using a simple sequential kinetic scheme with increasing lifetimes.

Three-dimensional surface plots of the data for acidic pH in the fingerprint region (1190–1300 cm^{-1}) and in the isomerization region (1450–1590 cm^{-1}), the IR spectral ranges in which the most significant changes take place, are shown in Fig. 3 *A*. The perturbed free induction decay affects the data during the first 0.1–0.2 ps (29), which is why the first lifetime is fixed to 0.2 ps.

Significantly, when fitting these data, we obtained very similar lifetimes as in the VIS pump-probe experiment: 0.2 ps, 1.4 ps, 26 ps, and a nondecaying component at pH 9.5 (data not shown) and 0.2 ps, 3 ps, 20 ps, and a nondecaying component at pH 6.5. The corresponding EADS (*upper panel*) and time traces (together with the fit to the data, *lower panel*) are shown in Fig. 3 for pH 6.5 (see Fig. 2S in the Supplementary Material, Data S1, for more time traces).

At both pH values, the main feature is the instantaneous bleaching of a band centered at 1534 cm^{-1} with a shoulder at 1550 cm^{-1}. The 1534 cm^{-1} band has been assigned to the C=C ethylenic stretch in the all-*trans* configuration (30). The positive features at 1475 cm^{-1}, 1575 cm^{-1}, and 1300 cm^{-1}

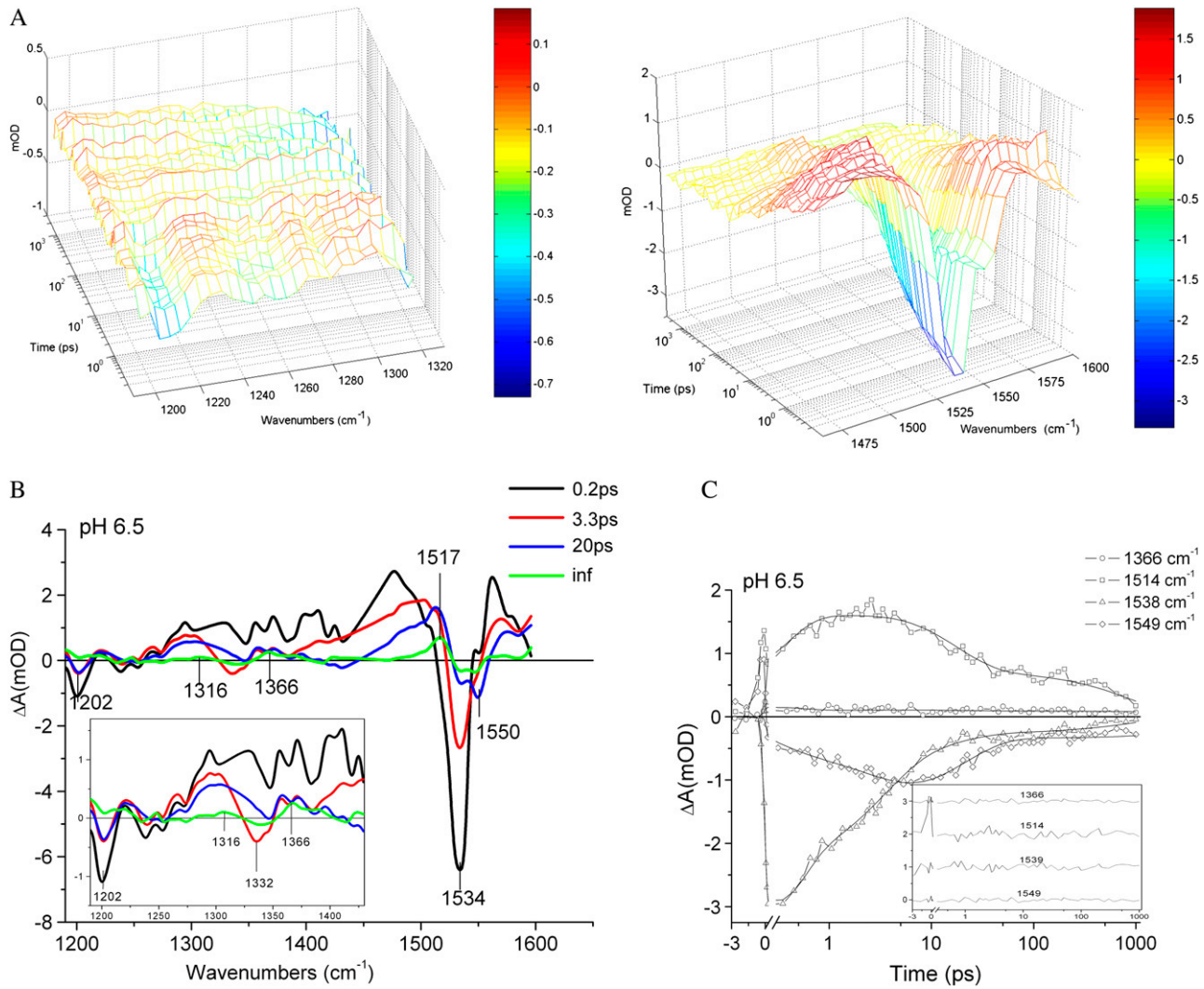

FIGURE 3 (*A*) Three-dimensional surface plots of the raw ultrafast transient IR absorption data at pH 6.5 in the spectral regions 1180–1300 cm^{-1} (*left*) and 1460–1600 cm^{-1} (*right*). (*B*) Time series of IR EADS derived from global analysis of the data set with a sequential model; the inset zooms in on the spectral region from 1190 to 1430 cm^{-1}. The time constant associated with each EADS is shown in the legend. (*C*) Time traces at selected wavelengths of the acidic (pH 6.5) sample together with the fit resulting from global analysis; residuals from the fit of every time trace are shown in the inset.

are caused by vibrational bands in the excited state. In general, bands in the excited state may be shifted to another frequency because of the different electron distribution or different conformation of the molecule in the excited state, but also, coupling to vibrationally hot states will, because of anharmonicity, lead to a red shift of the modes that will relax with the cooling of the molecule, typically in a few picoseconds (31). In ~0.2 ps, the 1475 cm^{-1} band decays and shifts to the blue, probably partially causing the concomitant decrease of the negative band at 1534 cm^{-1}. The bleaching at 1202 cm^{-1} and the induced absorption in the fingerprint region (1270–1330 cm^{-1}) are also decreasing on the subpicosecond timescale. After 3 ps, in addition to a further decay of the vibrationally hot bands and a decrease of the negative 1534 cm^{-1} band, a narrower feature at 1517 cm^{-1} can now be recognized, better separated from the broad band at 1475 cm^{-1} than at shorter times. In addition, a negative band ~1550 cm^{-1} develops. A further decay of the broad bands at 1475 and 1575 cm^{-1} occurs after 20 ps, together with a decrease of the negative bands at 1534 and 1550 cm^{-1}, leaving a small double-peaked negative signal at 1534 cm^{-1} and 1550 cm^{-1} and a positive feature at 1517 cm^{-1} during the window of observation.

The positive band centered at 1517 cm^{-1} has been assigned to the ethylenic stretch of isomerized 13-*cis* retinal (32). The final spectrum also shows small positive peaks at 1316 cm^{-1}, 1247 cm^{-1}, and 1216 cm^{-1}. The amplitude of the final spectrum, i.e., that of the K-state, is rather small. This may be partially a result of overlap of the ethylenic stretch bands in the ground state with those in the K-state, but it also reflects the ''less-than-unity'' quantum yield of isomerization.

Low-temperature IR difference spectra and time-resolved IR data of photoisomerizing proteins show that the amplitudes of the bands characteristic of the all-*trans* configuration (negative) are somewhat larger than the corresponding bands in the *cis* confugration. This ''asymmetry'' is observable in the spectra of photoactive yellow protein (27,33–35) and bacteriorhodopsin (36,37) and might be caused by different extinction coefficients of the bands in the *cis* configuration. However, the extinction coefficients of the C=C bands in the K-state of pR are fairly well matched (9).

In summary, the results of our VIS-VIS pump-probe and our VIS-mid-IR pump-probe studies yield very comparable time constants for the respective transitions at both pH values: 2 ps and 18 ps vs. 3 ps and 20 ps (pH 6.5) and 1 ps and 23 ps vs. 1.4 and 26 ps (pH 9.5), respectively (in addition to a 0.2-ps time constant that was fixed in all analyses). Our data are in fairly good qualitative agreement with earlier reports in the literature: In two recent studies, the Wachtveitl group (16,18) reported biphasic formation of the K-state in 0.3–0.4 ps and ~9 ps at pH 9 and 1 ps and 16 ps at pH 6, with the fast phase being more dominant at high pH than at low pH. Amsden et al. (18) reported time constants of 0.5 ps, 2 ps, and 11 ps in a VIS-IR study at pH 9.5, using an observation window of 30 ps. They assigned the 0.5-ps component to isomerization during the excited state plus an amide II backbone response and the 2-ps component to the formation of a *cis* ground-state isomer; the interpretation of the 11-ps component was not clear. The difference in measured rates between the studies of Lenz et al. at pH 9 and the current study on the one hand and that of Amsden et al. on the other may be caused by differences in sample preparation (16,18).

Because the time constants in our VIS and IR data are so similar, we can proceed to fit a specific model in a target analysis to the VIS and IR data simultaneously. This will allow us to 1), determine more quantitatively how much K-state is formed and on which timescale and 2), obtain the excited-minus-ground-state difference spectrum because, at most time delays, the measured spectrum is a time-evolving mixture of the excited state and the K-product state.

Target analysis

The visible data show that the regions of stimulated emission and excited state absorption decay with three time constants, and therefore, we include three excited states in our model plus a state that represents the K-product state. Initially we allowed for a sequential relaxation from ES1 to ES2 to ES3 and allowed for product formation from the later two states only. When we fit this model to our data, we found that the spectra of ES2 and ES3 are very similar. Therefore, we fitted a model in which we restricted the spectra of ES2 and ES3 to be identical in the VIS wavelength range but not in the IR. This yielded a good fit to the data if we also allowed a small fraction of product formation from ES1. This model is depicted in Fig. 4, and the corresponding rate constants are given in Table 1. For each state, we allow for product formation, relaxation to the next excited state, and decay to the electronic ground state(s). The sum of the corresponding rate constants is determined by the lifetime of each state, whereas the partitioning of the rates is mainly determined from the most physically meaningful mutual scaling of the resulting spectra. The resulting spectra (i.e., SADS) are depicted in Figs. 5 and 6. The first species, ES1, has a very short lifetime for both the acidic and the alkaline sample and is difficult to characterize because of the interference from xpm artifacts. Nevertheless, it seems there is stimulated emission at ~640 nm. This species relaxes to the excited state species denoted ES2 with a stimulated-emission shift to ~725 nm, indicating a movement of the initially excited state out of the Frank-Condon region on an ultrafast timescale, in agreement with earlier findings (16). ES2 is depopulated through fast, 1-ps, K-formation and through further relaxation to ES3. ES3 decays to the K-state and to the stable ground state in ~20 ps. The visible spectrum of the ES2 and ES3 states can be taken to be identical, but in the mid-IR, there is clear spectral evolution between these two excited-state intermediates. We further note that, at wavelengths above 640 nm, the stimulated emission at pH 9.5 is less than at lower pH.

The time-resolved IR (difference) spectrum of the isomerized K-state is in very good agreement with the corresponding low-temperature FTIR difference spectrum (10). In the mid-IR, the K-state spectrum is distinguishable from the ES2 and ES3 spectra by the narrow sharp band at 1517 cm^{-1}

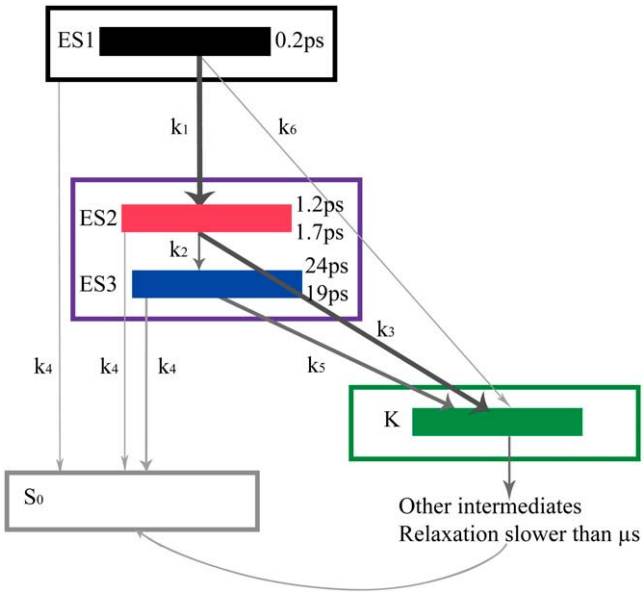

FIGURE 4 Schematic representation of the dynamics of the initial stages of the photocycle of pR. Lifetimes and rate constants are indicated. The outer squares are color coded to SADS in the visible (see Fig. 5), and the inner squares are color coded to the SADS in the mid-IR (see Fig. 6). The upper values correspond to the sample at pH 9.5; the lower values to pH 6.5. The values of the rate constants are given in Table 1.

TABLE 1 Rate constants of the transitions derived from the model depicted in Fig. 4

Decay rate	pH 9.5 (1/ps)	pH 6.5 (1/ps)
k_1 ES1 → ES2	5.0	5.0
k_2 ES2 → ES3	0.53	0.37
k_3 ES2 → K	0.25	0.16
k_4 ES1 → S_0; ES2 → S_0; ES3 → S_0	0.02	0.04
k_5 ES3 → K	0.02	0.01
k_6 ES1 → K	0.35	0.4

and the small positive band at 1316 cm^{-1}. The 1517 cm^{-1} band is a marker for the isomerized 13-*cis* configuration, according to the known correlation of the vibrational frequencies of retinal with visible absorption maxima, which connects the red-shifted K-state absorption with a lower-frequency absorption in the mid-IR (38). The band at 1316 cm^{-1} is characteristic for Asp absorption and most probably indicates rearrangement of the H-bonds of the retinal Schiff base with the residues that form the complex counterion, i.e., Asp^{97}, Asp^{227}, and a water molecule inside the chromophore binding pocket (see also Fig. 1 *C*). The bands at ~1190–1250 cm^{-1} are characteristic of retinal C-C stretching vibrations (39). The positive band at 1190 cm^{-1} in the spectrum of the K-species probably corresponds to the 1192 cm^{-1} band of the mixed C_{14}–C_{15} and C_{10}–C_{11} stretching vibration of the chromophore previously identified in resonance Raman studies, indicating that isomerization occurs around the C_{13}–C_{14} vinyl bond (40). The facts that we obtain a reliable K-state spectrum and, with a fairly simple description of the excited-state dynamics, can fit both the VIS and IR pump-probe data, give us confidence that our model captures the most essential physical events in the early stages of the pR photocycle.

We can now calculate that at pH 9.5, ~6% of the K-state is formed in 0.2 ps, ~30% in 1 ps, and another 30% in 24 ps. At pH 6.5, this is 7% in 0.2 ps, 30% in 1.7 ps, and 15% in 19 ps. These numbers add up to quantum yields of 0.66 and 0.52 at pH 9.5 and 6.5, respectively, in reasonable agreement with the earlier estimate based on the extinction coefficients of the retinal chromophore (see above).

DISCUSSION

The combined pump-probe studies in the VIS and IR parts of the spectrum show that the formation of the first transient ground-state photocycle intermediate of pR (i.e., the K-state) is multiphasic, occurring in about equal parts in ~2 ps and 20 ps and for a very small extent on a subpicosecond timescale.

After excitation, the reaction proceeds through the following stages: initial movement out of the excited Frank-Condon region in ~0.2 ps, followed by either fast K-formation in ~2 ps or a further relaxation in the excited state toward ES3, and slow-phase K-formation in ~20 ps. The visible spectra show no hint as to why the isomerization proceeds on these two different timescales, but because the IR spectra of ES2 and ES3 are different, we now discuss these in more detail.

The main features of the IR spectra are the bleaching of the band at 1534 cm^{-1}, assigned to the C=C ethylenic stretch in the all-*trans* configuration (30), and the appearance of a positive band at lower frequencies. In the K-spectrum, this band is at 1517 cm^{-1} and is recognized as a marker for the isomerized 13-*cis* ground state configuration (38). In the ES2 and ES3 states, the same band is present, but much wider and extending to much lower frequencies. The width and position of this band probably track the evolution along the isomerization reaction coordinate, but the formation of a vibrationally hot state and its subsequent cooling may also have an effect on this spectral evolution. With the transition from the ES2 to ES3 state, this band narrows, thus developing a peak at 1511 cm^{-1}, much like that of the K-ground state, showing that also in proteins that do not make the transition to the isomerized K-ground state on this timescale, the backbone structure of the retinal chromophore relaxes. With the relaxation from the ES2 to the ES3 state, a relatively large increase in the bleaching of the band at 1550 cm^{-1} is observed (see Figs. 3 and 6). This band is missing in the resonance Raman spectra of pR (40). In bacteriorhodopsin a similar band was attributed to an amide II response to isomerization (41). The appearance of a 1550 cm^{-1} band on a timescale on the order of tens of picoseconds was also observed for SRII (42) and halorhodopsin (43) and was interpreted as a relax-

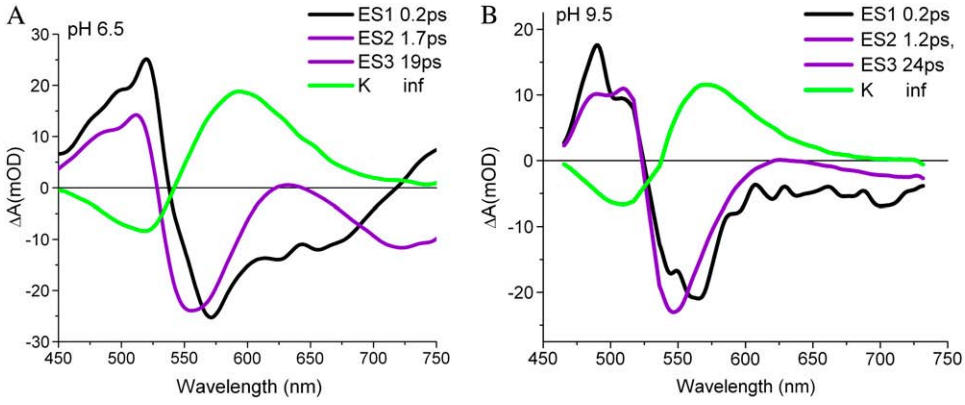

FIGURE 5 SADS in the visible derived from simultaneous global analysis with the target model shown in Fig. 4. (*A*) SADS at pH 6.5 from 450 to 750 nm. (*B*) SADS at pH 9.5 from 450 to 750 nm. Every species is associated with a lifetime, shown in the legend in the figure.

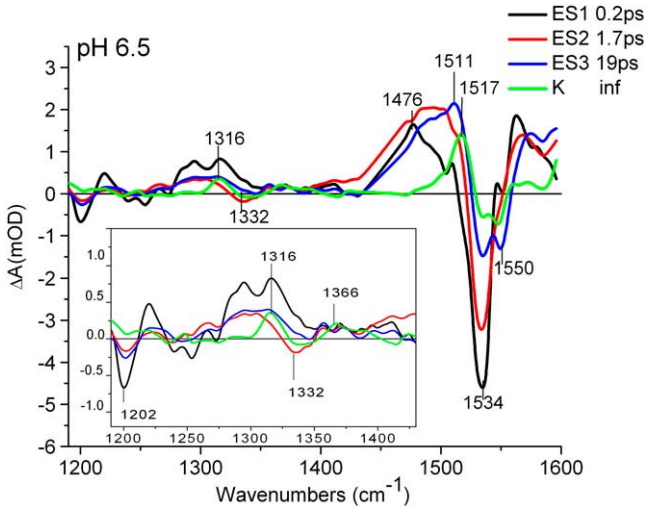

FIGURE 6 SADS in the mid-IR of the acidic sample in the spectral region 1190–1600 cm^{-1} derived from simultaneous global analysis with the target model shown in Fig. 4; the inset zooms in on the spectral region from 1190 to 1450 cm^{-1}.

ation of protein vibrational bands, possibly amide II bands of the protein backbone, perturbed by the ultrafast retinal photoisomerization. The kinetics of this band could not be well resolved in the global analysis but only in the kinetic analysis of single time traces, at 1554 cm^{-1} for bacteriorhodopsin and halorhodopsin and at 1550 cm^{-1} for sensory rhodopsin II, respectively (42,43). This band was observed to evolve together with a positive band centered ~1538 cm^{-1}, which we are not able to observe here, presumably because of overlap of the dominant bleaching of the all-*trans* ethylenic stretch at 1534 cm^{-1}. However, we observe a significant loss of signal in this band coinciding with the appearance of the 1550 cm^{-1} band in the ES3 state. In a recent study of pR by Amsden et al. (18), this negative band at 1548 cm^{-1} was also observed; these authors verified with selective isotope labeling that it can (at least partially) be assigned to an amide II peptide backbone mode. They reported that this mode appears almost coincident with the chromophore isomerization, with a time constant of 500–700 fs. Indeed, we find this band also to be present in our earliest spectra as a shoulder but to grow substantially with a time constant of 2 ps (see also Fig. 3 *C*) and, notably, to be present during the long-lived excited state of the retinal, i.e., in proteins that are slower in isomerization. The appearance of this band may result from the disappearance of an overlapping band but could also be an indication of the progression of either the isomerization process in the excited state, as sensed by the protein backbone, or of the protein relaxation itself. Molecular dynamics calculations (44) and FTIR spectroscopy of the 11-*cis*-locked analog of retinal in rhodopsin (45) show that the polarization change in the excited state of retinal could trigger a protein dielectric polarization relaxation on a picosecond timescale. Although this relaxation was calculated to occur on a picosecond timescale, it could lead to a conformational change of the protein, which might persist even after the chromophore has returned to the ground state (46). Apparently, the progressing response of the protein, as indicated by the bleaching of the 1550 cm^{-1} band, does not have a beneficial effect on the quantum yield of isomerization because the yield for the long-lived excited state is lower than that of the shorter-lived excited state ES2.

The bands in the region of 1350 to 1380 cm^{-1} have been shown to be dominated by the COO^- stretches of carboxylates (47,48). The FTIR K-minus-ground-state spectra of the pR mutants D97N, D97E, and D227E (49) show that the spectral changes in this region, dominated by the 11 cm^{-1} red shift of the band at 1389 cm^{-1}, are caused by Asp^{227} rather than Asp^{97}. In the spectrum of the K-state, we do observe a positive band at 1368 cm^{-1}; therefore, we attribute this band to Asp^{227} rather than Asp^{97} (49). We suppose that the 11 cm^{-1} difference in peak position between the current study and the low-temperature FTIR study is a result of the fact that our measurements are made at room temperature. The positive/negative feature at 1316/1332 cm^{-1} appearing in the K-state has not been assigned in previous IR and mutation studies of pR. A similar feature (at 1315/1328 cm^{-1}) was observed in later intermediates in the photocycle of bacteriorhodopsin and was proposed to be caused by the symmetric stretch of Asp^{212} (39). More study on pR mutants is needed for the assignment of this band, as it is not clear to what extent the Asp^{212} in bR corresponds to the Asp residues in proximity to the chromophore (i.e., Asp^{97} and Asp^{227}) in pR. The downshift of the Asp COO^- mode to 1368 cm^{-1} is in agreement with the suggestion that Asp^{227} becomes the H-bond partner of the Schiff base in the K-state (9).

Here we show that because changes are similar in the ES2, ES3, and K-state spectra, the interaction of this carboxylate with the chromophore is modified within 0.2 ps, probably by the altered electron distribution in the excited state(s) or by the early structural distortion of the chromophore in the excited state. At low pH (i.e., 6.5), the Schiff-base proton acceptor (Asp^{97}) is protonated. We observe that this has a moderate effect on the quantum yield of isomerization, which is ~0.7 at high pH and ~0.5 at slightly acidic pH, with the largest effect on the slow phase (~20 ps) of isomerization. Decrease of the isomerization rate of the D97N mutant of pR as compared with wild-type at pH 6 has been observed by ultrafast spectroscopy in the visible (17). From this we concluded (17) that steric hindrance of protonated Asp^{97} may play a role too, apart from changed electrostatic interactions, in the lower quantum yield at pH 6.5.

SUPPLEMENTARY MATERIAL

To view all of the supplemental files associated with this article, visit www.biophysj.org.

The authors thank Dr. K. H. Yung (Department of Life Science and Interdisciplinary Program of Integrated Biotechnology, Sogang University,

Shinsu-Dong, Mapo-Gu, Seoul, Korea) for making available to us the *E. coli* strain that allows overproduction of holo-pR. The authors thank Dr. Jocelyne Vreede (van 't Hoff Institute of Molecular Sciences, University of Amsterdam, Amsterdam, The Netherlands) for improving the homology model made available to us by Dr. O. Beja (Department of Biology, Technion-Israel Institute of Technology, Haifa, Israel), using the 3DJigsaw homology modeling and the SWISS-MODEL web server.

This research was supported by The Netherlands Organization for Scientific Research via the Dutch Foundation for Earth and Life Sciences (NWO-ALW) (investment grant 812.08.001 and MtC grant 805.47.123 to K.J.H.). M.L.G. is grateful to NWO-ALW for providing financial support with a long-term fellowship (grant 834.01.002).

REFERENCES

1. Beja, O., L. Aravind, E. V. Koonin, M. T. Suzuki, A. Hadd, L. P. Nguyen, S. Jovanovich, C. M. Gates, R. A. Feldman, J. L. Spudich, E. N. Spudich, and E. F. DeLong. 2000. Bacterial rhodopsin: Evidence for a new type of phototrophy in the sea. *Science*. 289:1902–1906.
2. Beja, O., E. N. Spudich, J. L. Spudich, M. Leclerc, and E. F. DeLong. 2001. Proteorhodopsin phototrophy in the ocean. *Nature*. 411:786–789.
3. Bryant, D. A., and N. U. Frigaard. 2006. Prokaryotic photosynthesis and phototrophy illuminated. *Trends Microbiol.* 14:488–496.
4. Walter, J. M., D. Greenfield, C. Bustamante, and J. Liphardt. 2007. Light-powering *E. coli* with proteorhodopsin. *Proc. Natl. Acad. Sci. USA*. 104:2408–2412.
5. Man, D. L., W. W. Wang, G. Sabehi, L. Aravind, A. F. Post, R. Massana, E. N. Spudich, J. L. Spudich, and O. Beja. 2003. Diversification and spectral tuning in marine proteorhodopsins. *EMBO J*. 22:1725–1731.
6. Hillebrecht, J. R., J. Galan, R. Rangarajan, L. Ramos, K. McCleary, D. E. Ward, J. A. Stuart, and R. R. Birge. 2006. Structure, function, and wavelength selection in blue-absorbing proteorhodopsin. *Biochemistry*. 45:1579–1590.
7. Spudich, J. L. 2006. The multitalented microbial sensory rhodopsins. *Trends Microbiol*. 14:480–487.
8. Dioumaev, A. K., L. S. Brown, J. Shih, E. N. Spudich, J. L. Spudich, and J. K. Lanyi. 2002. Proton transfers in the photochemical reaction cycle of proteorhodopsin. *Biochemistry*. 41:5348–5358.
9. Ikeda, D., Y. Furutani, and H. Kandori. 2007. FTIR study of the retinal Schiff base and internal water molecules of proteorhodopsin. *Biochemistry*. 46:5365–5373.
10. Varo, G., L. S. Brown, M. Lakatos, and J. K. Lanyi. 2003. Characterization of the photochemical reaction cycle of proteorhodopsin. *Biophys. J*. 84:1202–1207.
11. Lakatos, M., J. K. Lanyi, J. Szakacs, and G. Varo. 2003. The photochemical reaction cycle of proteorhodopsin at low pH. *Biophys. J*. 84:3252–3256.
12. Dioumaev, A. K., J. M. Wang, Z. Balint, G. Varo, and J. K. Lanyi. 2003. Proton transport by proteorhodopsin requires that the retinal Schiff base counterion Asp-97 be anionic. *Biochemistry*. 42:6582–6587.
13. Friedrich, T., S. Geibel, R. Kalmbach, I. Chizhov, K. Ataka, J. Heberle, M. Engelhard, and E. Bamberg. 2002. Proteorhodopsin is a light-driven proton pump with variable vectoriality. *J. Mol. Biol*. 321: 821–838.
14. Imasheva, E. S., S. P. Balashov, J. M. Wang, A. K. Dioumaev, and J. K. Lanyi. 2004. Selectivity of retinal photoisomerization in proteorhodopsin is controlled by aspartic acid 227. *Biochemistry*. 43:1648–1655.
15. Huber, R., T. Kohler, M. O. Lenz, E. Bamberg, R. Kalmbach, M. Engelhard, and J. Wachtveitl. 2005. pH-dependent photoisomerization of retinal in proteorhodopsin. *Biochemistry*. 44:1800–1806.
16. Lenz, M. O., R. Huber, B. Schmidt, P. Gilch, R. Kalmbach, M. Engelhard, and J. Wachtveitl. 2006. First steps of retinal photoisomerization in proteorhodopsin. *Biophys. J*. 91:255–262.
17. Lenz, M., A. C. Woerner, C. Glaubitz, and J. Wachtveitl. 2007. Photoisomerization in proteorhodopsin mutant D97N. *Photochem. Photobiol*. 83:226–231.
18. Amsden, J. J., J. M. Kralj, L. R. Chieffo, X. Wang, S. Erramilli, E. N. Spudich, J. L. Spudich, L. D. Ziegler, and K. J. Rothschild. 2007. Subpicosecond protein backbone changes detected during the green-absorbing proteorhodopsin primary photoreaction. *J. Phys. Chem. B*. 111:11824–11831.
19. Imasheva, E. S., K. Shimono, S. P. Balashov, J. M. Wang, U. Zadok, M. Sheves, N. Kamo, and J. K. Lanyi. 2005. Formation of a long-lived photoproduct with a deprotonated Schiff base in proteorhodopsin, and its enhancement by mutation of Asp227. *Biochemistry*. 44:10828–10838.
20. Bergo, V., J. J. Amsden, E. N. Spudich, J. L. Spudich, and K. J. Rothschild. 2004. Structural changes in the photoactive site of proteorhodopsin during the primary photoreaction. *Biochemistry*. 43: 9075–9083.
21. van Stokkum, I. H. M., D. S. Larsen, and R. van Grondelle. 2004. Global and target analysis of time-resolved spectra. *Biochim. Biophys. Acta*. 1657:82–104.
22. Contreras-Moreira, B., and P. A. Bates. 2002. Domain fishing: a first step in protein comparative modelling. *Bioinformatics*. 18:1141–1142.
23. Patzelt, H., B. Simon, A. terLaak, B. Kessler, R. Kuhne, P. Schmieder, D. Oesterhelt, and H. Oschkinat. 2002. The structures of the active center in dark-adapted bacteriorhodopsin by solution-state NMR spectroscopy. *Proc. Natl. Acad. Sci. USA*. 99:9765–9770.
24. Schwede, T., J. Kopp, N. Guex, and M. C. Peitsch. 2003. SWISS-MODEL: an automated protein homology-modeling server. *Nucleic Acids Res*. 31:3381–3385.
25. Gergely, C., L. Zimanyi, and G. Varo. 1997. Bacteriorhodopsin intermediate spectra determined over a wide pH range. *J. Phys. Chem. B*. 101:9390–9395.
26. Tittor, J., and D. Oesterhelt. 1990. The quantum yield of bacteriorhodopsin. *FEBS Lett*. 263:269–273.
27. van Wilderen, L. J. G. W., M. A. van der Horst, I. H. M. van Stokkum, K. J. Hellingwerf, R. van Grondelle, and M. L. Groot. 2006. Ultrafast infrared spectroscopy reveals a key step for successful entry into the photocycle for photoactive yellow protein. *Proc. Natl. Acad. Sci. USA*. 103:15050–15055.
28. Oesterhelt, D., P. Hegemann, and J. Tittor. 1985. The photocycle of the chloride pump halorhodopsin. 2. quantum yields and a kinetic-model. *EMBO J*. 4:2351–2356.
29. Hamm, P. 1995. Coherent effects in femtosecond infrared spectroscopy. *Chem. Phys*. 200:415–429.
30. Bagley, K., G. Dollinger, L. Eisenstein, A. K. Singh, and L. Zimanyi. 1982. Fourier-transform infrared difference spectroscopy of bacteriorhodopsin and its photoproducts. *Proc. Natl. Acad. Sci. USA*. 79:4972–4976.
31. Nibbering, E. T. J., H. Fidder, and E. Pines. 2005. Ultrafast chemistry: Using time-resolved vibrational spectroscopy for interrogation of structural dynamics. *Annu. Rev. Phys. Chem*. 56:337–367.
32. Hackmann, C., J. Guijarro, I. Chizhov, M. Engelhard, C. Rodig, and F. Siebert. 2001. Static and time-resolved step-scan Fourier transform infrared investigations of the photoreaction of halorhodopsin from *Natronobacterium pharaonis*: Consequences for models of the anion translocation mechanism. *Biophys. J*. 81:394–406.
33. Groot, M. L., L. J. G. W. vanWilderen, D. S. Larsen, M. A. vanderHorst, I. H. M. vanStokkum, K. J. Hellingwerf, and R. vanGrondelle. 2003. Initial steps of signal generation in Photoactive Yellow Protein revealed with femtosecond mid-infrared spectroscopy. *Biochemistry*. 42:10054–10059.
34. Heyne, K., O. F. Mohammed, A. Usman, J. Dreyer, E. T. J. Nibbering, and M. A. Cusanovich. 2005. Structural evolution of the chromophore

in the primary stages of *trans*/*cis* isomerization in photoactive yellow protein. *J. Am. Chem. Soc.* 127:18100–18106.

35. Imamoto, Y., Y. Shirahige, F. Tokunaga, T. Kinoshita, K. Yoshihara, and M. Kataoka. 2001. Low-temperature Fourier transform infrared spectroscopy of Photoactive Yellow Protein. *Biochemistry.* 40:8997–9004.
36. Herbst, J., K. Heyne, and R. Diller. 2002. Femtosecond infrared spectroscopy of bacteriorhodopsin chromophore isomerization. *Science.* 297: 822–825.
37. Rammelsberg, R., G. Huhn, M. Lubben, and K. Gerwert. 1998. Bacteriorhodopsin's intramolecular proton-release pathway consists of a hydrogen-bonded network. *Biochemistry.* 37:5001–5009.
38. Kakitani, H., T. Kakitani, H. Rodman, B. Honig, and R. Callender. 1983. Correlation of vibrational frequencies with absorption maxima in polyenes, rhodopsin, bacteriorhodopsin, and retinal analogs. *J. Phys. Chem.* 87:3620–3628.
39. Rothschild, K. J., M. S. Braiman, Y. W. He, T. Marti, and H. G. Khorana. 1990. Vibrational spectroscopy of bacteriorhodopsin mutants—evidence for the interaction of aspartic-acid 212 with tyrosine 185 and possible role in the proton pump mechanism. *J. Biol. Chem.* 265:16985–16991.
40. Krebs, R. A., D. Dunmire, R. Partha, and M. S. Braiman. 2003. Resonance Raman characterization of proteorhodopsin's chromophore environment. *J. Phys. Chem. B.* 107:7877–7883.
41. Kluge, T., J. Olejnik, L. Smilowitz, and K. J. Rothschild. 1998. Conformational changes in the core structure of bacteriorhodopsin. *Biochemistry.* 37:10279–10285.
42. Diller, R., R. Jakober, C. Schumann, F. Peters, J. P. Klare, and M. Engelhard. 2006. The *trans-cis* isomerization reaction dynamics in sensory rhodopsin II by femtosecond time-resolved midinfrared spectroscopy: chromophore and protein dynamics. *Biopolymers.* 82:358–362.
43. Peters, F., J. Herbst, J. Tittor, D. Oesterhelt, and R. Diller. 2006. Primary reaction dynamics of halorhodopsin, observed by sub-picosecond IR–vibrational spectroscopy. *Chem. Phys.* 323:109–116.
44. Xu, D., C. Martin, and K. Schulten. 1996. Molecular dynamics study of early picosecond events in the bacteriorhodopsin photocycle: dielectric response, vibrational cooling and the J, K intermediates. *Biophys. J.* 70:453–460.
45. Fan, G., F. Siebert, M. Sheves, and R. Vogel. 2002. Rhodopsin with 11-*cis*-locked chromophore is capable of forming an active state photoproduct. *J. Biol. Chem.* 277:40229–40234.
46. Haupts, U., J. Tittor, and D. Oesterhelt. 1999. Closing in on bacteriorhodopsin: progress in understanding the molecule. *Annu. Rev. Biophys. Biomol. Struct.* 28:367–399.
47. Barth, A., and C. Zscherp. 2000. Substrate binding and enzyme function investigated by infrared spectroscopy. *FEBS Lett.* 477:151–156.
48. Dioumaev, A. K. 2001. Infrared methods for monitoring the protonation state of carboxylic amino acids in the photocycle of bacteriorhodopsin. *Biochemistry (Mosc.).* 66:1269–1276.
49. Furutani, Y., D. Ikeda, M. Shibata, and H. Kandori. 2006. Strongly hydrogen-bonded water molecule is observed only in the alkaline form of proteorhodopsin. *Chem. Phys.* 324:705–708.
50. Lakatos, M., and G. Varo. 2004. The influence of water on the photochemical reaction cycle of proteorhodopsin at low and high pH. *J. Photochem. Photobiol. B.* 73:177–182.